**CERN-ACC-NOTE-2021-0003**

11.01.2021

Hannes.Bartosik@cern.ch

# Space charge and intrabeam scattering effects for Lead-ions and Oxygen-ions in the LHC injector chain

I. John, Lund University, Sweden
H. Bartosik, CERN, CH-1211 Geneva, Switzerland

Keywords: Pb ions, O ions, LHC injector chain, SPS, space charge, intrabeam scattering, beam losses, simulation

Abstract

In the context of a possible LHC run with Oxygen-ion beams in about 2023, this report presents results of the space charge and intrabeam scattering effects for the Oxygen beam in comparison to the operational Lead beam in the LHC ion-injector chain (LEIR, PS and SPS).

Analytical calculations of the space charge tune shift indicate no limitations for an Oxygen beam in LEIR and PS as the tune shifts are smaller for Oxygen than for Lead. However, the tune shift for Oxygen is large in the SPS and thus macroparticle simulations (frozen and self-consistent) are performed to study the space charge effects on the Oxygen beam. These simulations predict a fast emittance blow-up of the Oxygen beam by about a factor of two, which might result in particle loss on the machine aperture. It is suggested to consider bunch splitting in the PS to reduce the intensity per bunch in the SPS. No limitations from intrabeam scattering are expected for the Oxygen beam, since the emittance growth calculated with numerical and analytical intrabeam scattering methods is much smaller for the Oxygen beam than for the Lead beam in all three injectors.

# Contents

# 1 Introduction

The work presented here is done in the context of the Oxygen Working Group, in preparation for a possible physics run with Oxygen-ions in the LHC in about 2023. Space charge and intrabeam scattering effects and possible limitations to be expected in the LHC ion injector chain (LEIR, PS, and SPS) are discussed.

Oxygen beams are of interest as they are intermediate in size between protons and Lead ions, presently used for physics runs at the LHC [1]. This work focuses on investigating the effects of space charge and intrabeam scattering on a beam of Oxygen-ions. The Lead beam is used as a reference to compare the Oxygen results. The Oxygen beam uses the same injector chain as used for the Lead beam production: After the extraction of the ions from a source, they are first accelerated in LINAC3, from which they are injected into LEIR as a partially stripped coasting beam. In LEIR, the beam is cooled to decrease the emittances and, after RF capture into one or two bunches, accelerated and extracted towards the PS. Depending on the beam production schemes, the bunches can be split in the PS and at the PS-to-SPS transfer the beam is fully stripped. The ions are accelerated to LHC injection energy in the SPS [1, 2].

This paper is organised as follows. Section 2 focuses on the effects of space charge (SC). The tune shift due to space charge is evaluated analytically, and macroparticle simulations are used to study the emittance growth in the SPS over many turns in the accelerator. The effects of intrabeam scattering (IBS) are investigated in Section 3. Analytical and numerical calculations are used to determine the effects of IBS on the emittance and bunch length of the beam. In Section 4, the methods from Sections 2 and 3 are used to compare the calculated and simulated emittance evolution due to space charge and intrabeam scattering with emittance measurements of a Lead beam in the SPS performed in 2016. The obtained beam size is compared to the aperture of SPS in Section 5. A summary of the main results and conclusions are given in Section 6. Appendix A provides additional information and a comparison of the different simulation models used. In Appendix B the analytically expected space charge induced tune shift is compared to the results from simulations.

# 2 Space charge effects

This section shows the results of the space charge effects on an Oxygen (O) beam in comparison to a Lead (Pb) beam. In Section 2.1, the parameters and assumptions used to calculate the space charge effects are given. In Section 2.2, the transverse tune shifts are presented. The tune spread is further investigated for the case of the SPS with several types of macroparticle simulations (frozen and self-consistent space charge solvers) to investigate the long-term effects of space charge on the beam in the accelerator, which can be found in Section 2.3. The different simulation methods are compared in Appendix A.

## 2.1 Space charge

Space charge (SC) is a collective effect which refers to the electromagnetic fields generated by the charged particles in an accelerator. In general, these induced electromagnetic fields cause interactions of the bunch of charged particles with the close surrounding material,

e.g. the vacuum chambers (referred to as indirect space charge), but also among the particles themselves even in the absence of surrounding materials (referred to as direct space charge) [3]. Space charge effects are strongest and most important at injection and lower energies. In the injectors of the LHC, the direct space charge effect is orders of magnitude bigger compared to the indirect space charge, at least at the corresponding injection energy in each machine. Therefore this paper is focused on direct space charge only. The induced tune shift in combination with lattice resonances can result in emittance growth and losses [4].

## 2.2 Analytical calculation of tune shift

The transverse tune shifts $\Delta Q_x$ and $\Delta Q_y$ resulting from direct space charge can be analytically calculated as [4]

$$\begin{aligned} \Delta Q_x &= -\frac{r_0 \lambda}{2\pi e \beta^2 \gamma^3} \oint \frac{\beta_x(s)}{\sigma_x(s)\left(\sigma_x(s)+\sigma_y(s)\right)} ds, \\ \Delta Q_y &= -\frac{r_0 \lambda}{2\pi e \beta^2 \gamma^3} \oint \frac{\beta_y(s)}{\sigma_y(s)\left(\sigma_x(s)+\sigma_y(s)\right)} ds, \end{aligned} \tag{1}$$

where $\Delta Q_x$ and $\Delta Q_y$ are the tune shift in the horizontal and vertical plane, respectively, and the transverse beam sizes $\sigma_x$ and $\sigma_y$ are given by

$$\begin{aligned} \sigma_x(s) &= \sqrt{\beta_x(s)\,\varepsilon_x/(\beta\gamma) + D_x^2(s)\left(\frac{\delta p}{p}\right)^2}, \\ \sigma_y(s) &= \sqrt{\beta_y(s)\,\varepsilon_y/(\beta\gamma)}, \end{aligned} \tag{2}$$

where the normalised emittances in the horizontal and vertical plane are given by $\varepsilon_x$ and $\varepsilon_y$, respectively, $\beta_x(s)$ and $\beta_y(s)$ are the optical beta functions, $D_x$ is the dispersion in the horizontal plane, and $\sigma_z$ is the rms bunch length. The classical particle radius $r_0$ is given by

$$r_0 = \frac{(n_q e)^2}{4\pi\epsilon_0 m},$$

with the number of charges $n_q$, the mass $m$ of the ion, the elementary charge $e$, and the vacuum permittivity $\epsilon_0$. The maximum line density $\lambda$, assuming a Gaussian shape, is determined by

$$\lambda = \frac{N_b e}{\sqrt{2\pi}\sigma_z},$$

where $N_b$ is the intensity of the beam (number of ions per bunch).

The tune shift is larger for smaller emittance and for lower energy, i.e. just after injection of the bunch into the accelerator. Therefore the initial parameters at injection are used to calculate the tune shifts. A summary with all the input parameters and calculated tune shifts for Pb and O beams considered here can be found in Table 1. The values for Pb beams are taken from [2, 5], while the values for O beams are taken from [1] or when unknown (e.g. the emittances) they are assumed to be the same as for Pb as an estimate. In LEIR, there are two bunches from seven injections for Pb ("nominal beam"), and one bunch from one injection for O ("Early beam").

Table 1: Summary table for beam parameters and tune shifts.

| | LEIR | | PS | | SPS | |
|---|---|---|---|---|---|---|
| | Pb | O | Pb | O | Pb | O |
| $\varepsilon_x$ [$10^{-6}$ m] | 0.4 (3) | 0.4 (4) | 0.8 (2) | 0.8 (4) | 1.3 (3) | 1.3 (4) |
| $\varepsilon_y$ [$10^{-6}$ m] | 0.4 (3) | 0.4 (4) | 0.5 (2) | 0.5 (4) | 0.9 (3) | 0.9 (4) |
| $\Delta p/p$ [$10^{-3}$] | 1.18 | 1.18 (4) | 0.63 | 0.63 (4) | 1 | 1 (4) |
| $N_b$ [$10^8$] | 10 (2) | 110 (1) | 8.1 (2) | 88 (1) | 3.5 (2) | 50 (1) |
| $n_q$ | 54 (2) | 4 (1) | 54 (2) | 4 (1) | 82 (2) | 8 (1) |
| $\sigma_z$ [m] | 4.256 | 8.5 (4) | 4.74 | 4.74 (4) | 0.23 | 0.23 (4) |
| $E_{\mathrm{kin}}/u$ [GeV] | 0.0042 (2) | 0.0042 (1) | 0.072 (2) | 0.0672 (1) | 5.9 (2) | 5.63 (1) |
| $m$ [GeV] | 193.8 | 14.9 | 193.8 | 14.9 | 193.8 | 14.9 |
| $B\rho$ [Tm] | 1.14 | 1.18 | 4.81 | 4.81 | 57.4 | 43.4 |
| $\beta$ | 0.09464 | 0.09464 | 0.3720 | 0.3606 | 0.9907 | 0.9899 |
| $\gamma$ | 1.00451 | 1.00451 | 1.0773 | 1.07214 | 7.33391 | 7.04405 |
| $\Delta Q_x$ | −0.35 | −0.14 | −0.24 | −0.19 | −0.20 | −0.38 |
| $\Delta Q_y$ | −0.31 | −0.12 | −0.3 | −0.24 | −0.29 | −0.55 |

References:
(1) ref. [1]
(2) ref. [2]
(3) ref. [5]
(4) if not known for O, assuming same as for corresponding Pb beam

Figure 1 shows the calculated tune shifts in the three injectors for Pb and O. In LEIR and PS, the tune shifts due to direct space charge are smaller for O than for Pb, and thus space charge is not expected to be a limitation for O beams in these machines. However, the tune shifts in the SPS for O are larger than for Pb, and especially the vertical tune shift of −0.55 is quite large and almost double compared to Pb. In the SPS only a single injection from the PS will be used for the O beam, and thus the beam does not have to be stored as long as it is the case for the Pb beam (usually up to 14 injections in the SPS and thus flat bottom storage times of several tens of seconds). Nevertheless, since the tune shift is so large, this case is further investigated to determine what long-term effects are caused by the large tune shift for O beams.

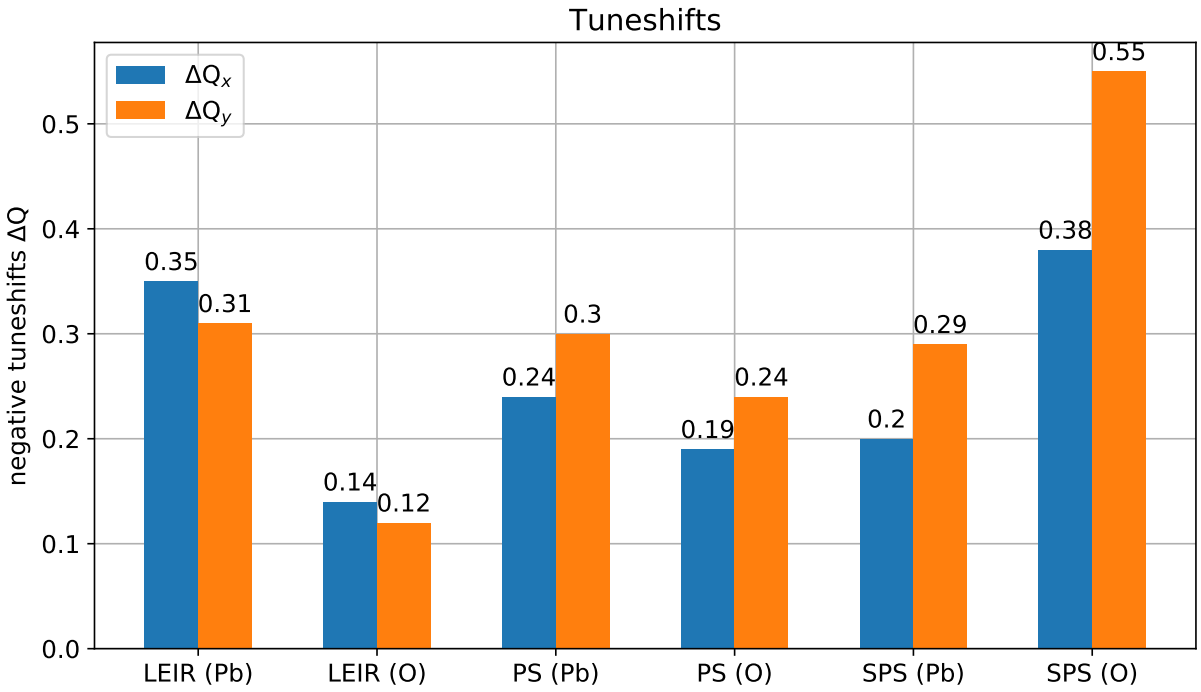


Figure 1: Analytically calculated tune shifts for Pb and O in LEIR, PS and SPS.

## 2.3 Space charge macroparticle simulations in SPS

Space charge simulations are performed to study the long-term effects of space charge in the SPS on the evolution of the tune shift and emittance. The PTC-Orbit code is used for these studies. In particular, the following three types of models are used: a frozen space charge solver and two self-consistent space charge solvers, called 2.5D and slice-by-slice (sbs). The results shown in this section are from the frozen model and the slice-by-slice self-consistent model. More information about the simulation models and more detailed comparisons between the models, also with the 2.5D self-consistent space charge solver, can be found in Appendix A.

For all simulations, the parameters as given in Table 1 are used, together with the 2018 lattice for SPS. The simulations are done for Pb and O. Usually, the frozen model considers 200 000 turns which corresponds to about 4.8 s in the SPS, while the self-consistent simulations are done for 10 000 turns, corresponding to about 0.24 s. In Section 2.3.2, the ideal lattice is considered, while later a quadrupole error is introduced in the lattice, as shown in Section 2.3.3.

### 2.3.1 Comparison to analytical tune shifts

To compare the analytically calculated tune shifts from Section 2.2 to the ones obtained from the simulations, the tune footprint is taken from the simulation after the first turns. Figure 2 shows the tune footprints for Pb and O obtained from the slice-by-slice model. In the tune diagrams, the green marker indicates the bare tune, which is the tune at zero intensity, here $Q_x = 26.30$ and $Q_y = 26.25$ as usually used for ion beams in the SPS in order to minimise

losses and emittance growth. As already expected by the analytically calculated tune shifts in Section 2.2, the tune spread is much larger for O than for Pb. There is good agreement between the analytical and numerical tune shift.

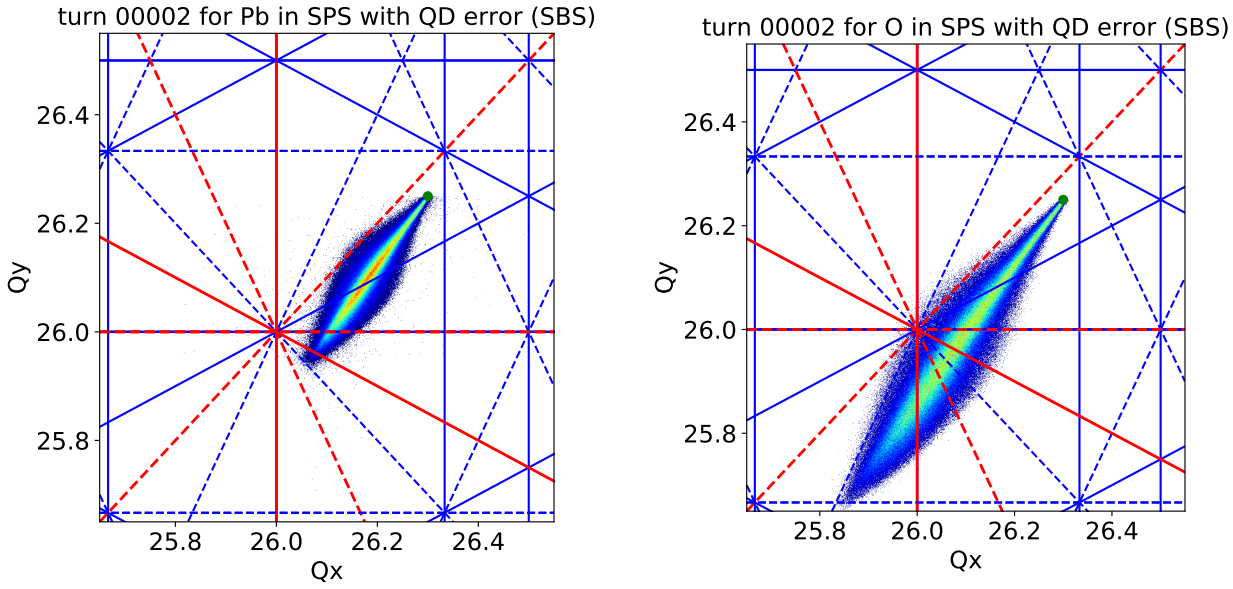


Figure 2: Tune footprint of SPS at injection for Pb (left) and O (right). The green dot indicates the bare tune.

### 2.3.2 Space charge simulations for the ideal SPS lattice

In this section, results from space charge simulations assuming an ideal SPS lattice (i.e. without imperfections) are presented. Figure 3 shows the emittance evolution and intensity for Pb (left) and O (right), comparing the frozen model and the slice-by-slice self-consistent space charge solver. The frozen model is shown for 200 000 turns, using 1 000 macroparticles, and the slice-by-slice model for about 4 000 turns, using 1 000 000 macroparticles. Figure 4 shows also the emittance evolution for Pb and O, but this time zoomed in to the first 10 000 turns.

For both the Pb and the O beam, the initial horizontal emittance is set to $\varepsilon_x = 1.3$ $\mu$m (normalised). In the case of Pb in the frozen model, the initial emittance appears to be larger (around $\varepsilon_x = 1.4$ $\mu$m) which is likely a numerical effect of the simulation since the number of macroparticles is relatively small (1 000). Besides that, the emittance for Pb remains relatively constant with only a small decrease in the horizontal plane. For O, the emittance increases, especially in the vertical plane, which is also consistent with the large tune shift $\Delta Q_y$. Here, the self-consistent space charge solver indicates an emittance growth stronger than given by the frozen model. The actual emittance growth lies probably between the emittances given by the two models. Since the frozen model is not fully self-consistent, it is possible that the calculated emittance growth is too small in the ideal lattice. However, this emittance growth is relatively small over 10 000 turns.

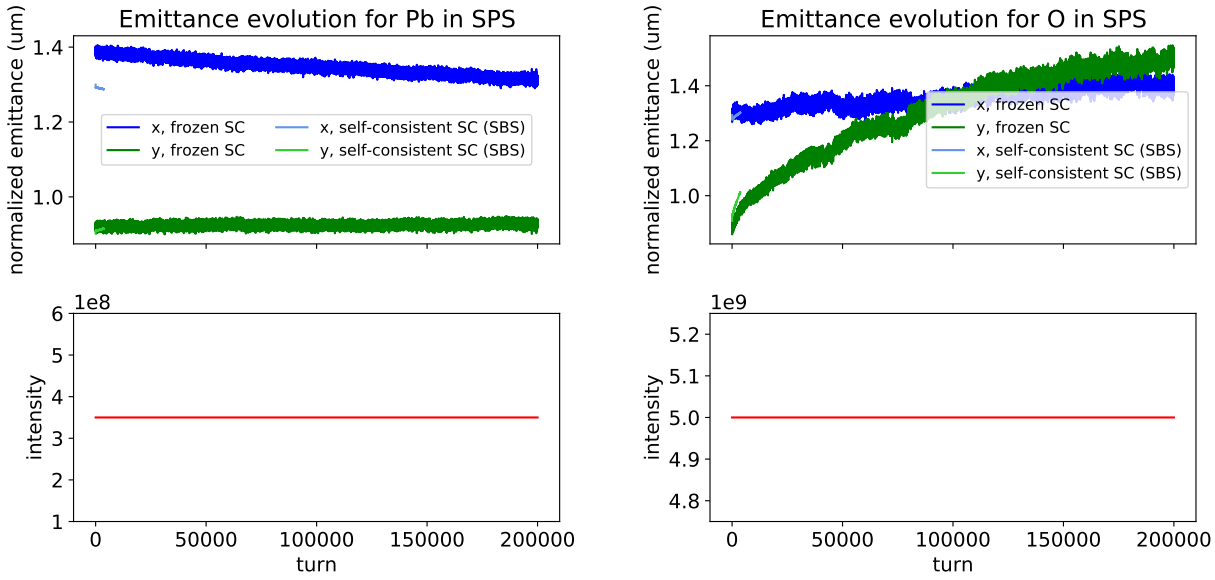


Figure 3: Comparison of the emittance evolution of the frozen model and slice-by-slice model for the Pb beam (left) and the O beam (right). For a zoomed-in version focusing on the slice-by-slice model, see figure 4.

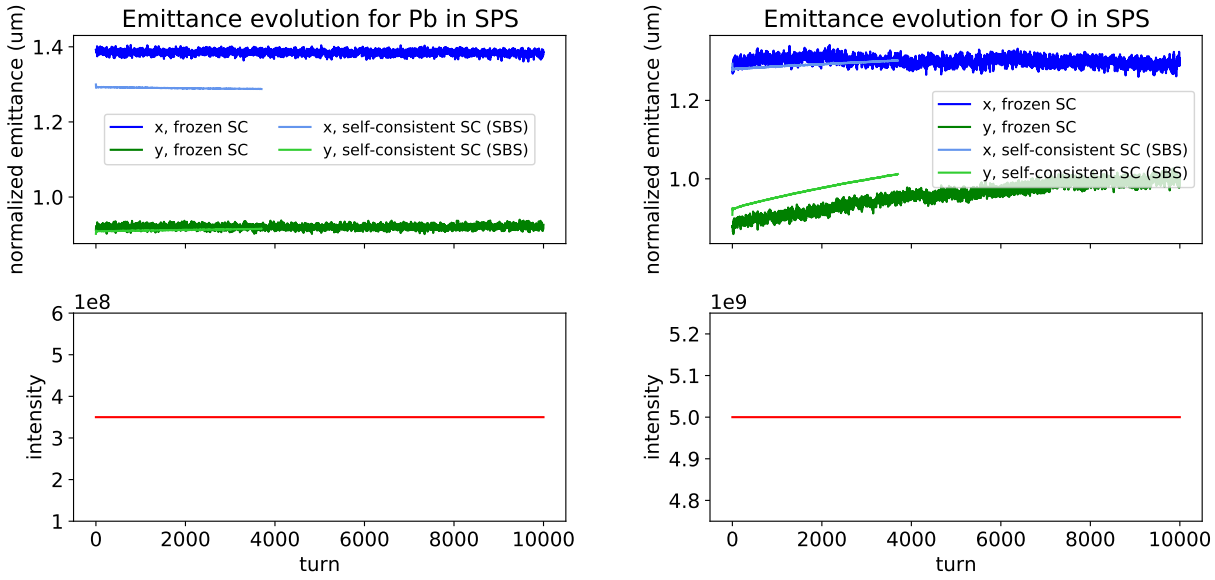


Figure 4: Comparison of the emittance evolution of the frozen model and slice-by-slice model for the Pb beam (left) and the O beam (right).

Examples of the bunch length evolution are given in Fig. 5 for O for the three simulations. The overall growth of the bunch length is small in the frozen case, and very small in the self-consistent cases.

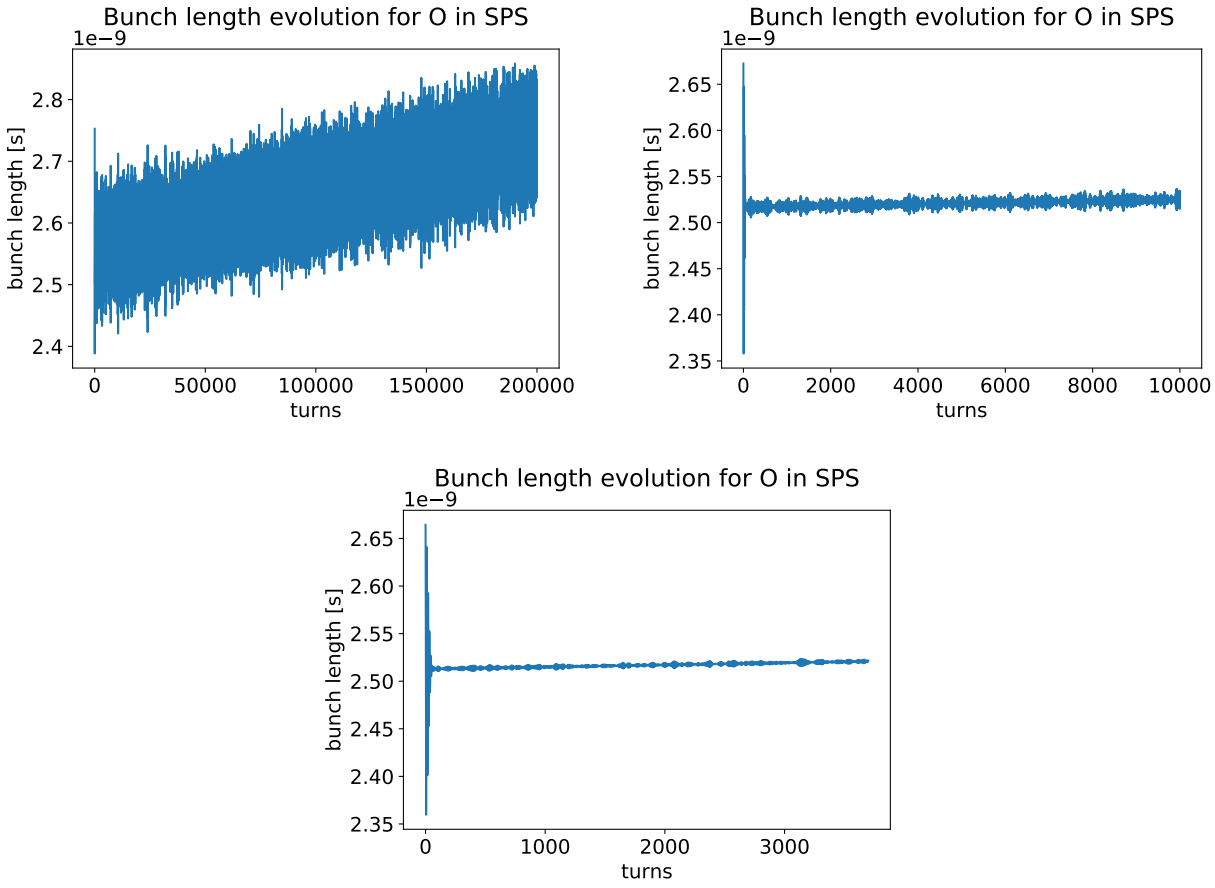


Figure 5: Bunch length evolution for the O beam in the frozen model (top left), for the 2.5D model (top right) and for the slice-by-slice model (bottom) for the ideal lattice.

### 2.3.3 Space charge simulations with quadrupole error

Imperfections are unavoidable in a real machine. To simulate a more realistic case compared to the ideal unperturbed SPS lattice, a quadrupole error of $\Delta k_1 = 0.0006$ m$^{-2}$ is introduced for a single defocusing quadrupole (QD). The error is chosen so that the amplitude of the vertical $\beta$ function increases by 10% maximum, which results in a horizontal increase of 2%. Figure 6 shows the behaviour of the $\beta$ functions without and with the quadrupole error, while in the latter case beta-beating can be observed due to the beam envelope being distorted. Quadrupole errors excite envelope resonances at integer and half-integer tunes.

For Pb, the emittance evolution is given in Fig. 7, comparing the ideal lattice to the lattice including the QD error, for the frozen model (left) and the slice-by-slice model (right). As can be seen, the effect of the QD error is small in the case of Pb. Both with and without the quadrupole error, there is a small exchange of emittance between the horizontal and vertical planes. In the case without error, there is even a small decrease of the average transverse emittance due to an exchange with the longitudinal plane (bunch lengthening). On the other hand, with the quadrupole error the average transverse emittance is slightly growing. From the left tune shift diagram in Fig. 2, it can be seen that in the case of Pb, the tune

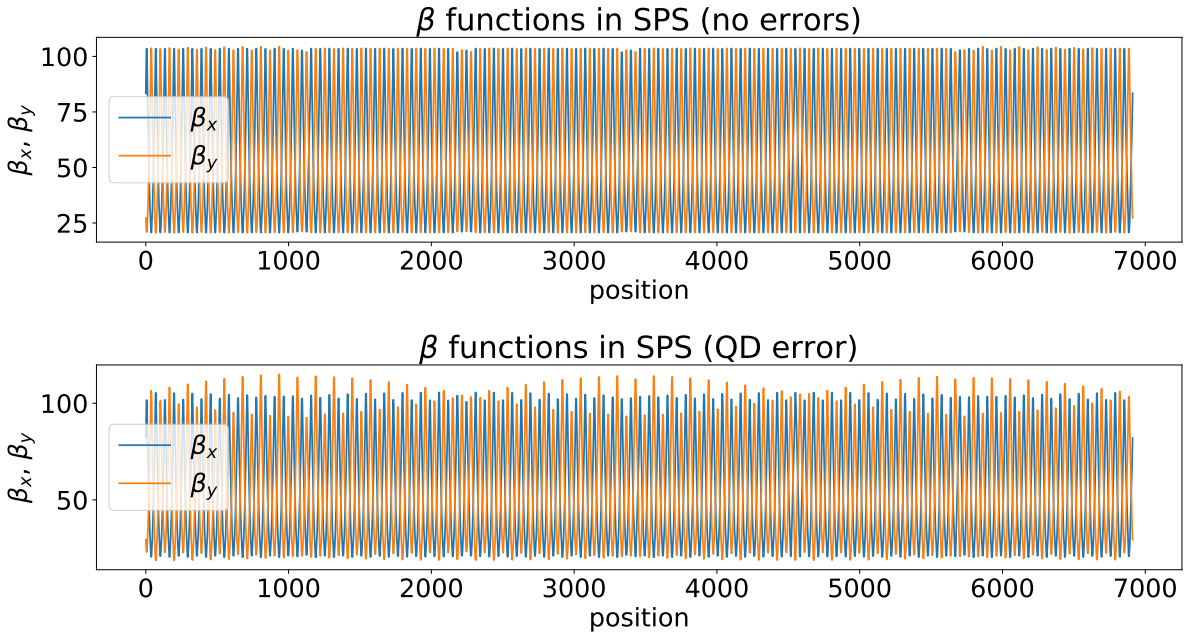


Figure 6: The horizontal and vertical $\beta$ functions of the SPS lattice without (top plot) and with (bottom plot) quadrupole error.

shift crosses the integer resonance in the vertical but not in the horizontal direction. This explains the emittance growth in the vertical plane in the presence of the error, compared to the constant vertical emittance in the case without quadrupole error. In the horizontal direction, there is almost no difference between the cases with and without QD error.

The emittance evolution with the quadrupole error for O is shown in Fig. 8, comparing the frozen model to the slice-by-slice SC solver. The left plot shows the evolution for the full number of turns, and the right plot shows the evolution zoomed in to the first 1 000 turns, as this is where most of the emittance growth happens. The two simulation models agree within their limitations (non-self consistency for the frozen model, additional emittance growth due to numerical noise for the slice-by-slice solver) and both show that the blow-up is very fast in the first 400 turns. As shown in the tune footprint for O in Fig. 2, the tune shift crosses both integer resonances in the horizontal and vertical planes, resulting in an emittance increase in both transverse directions.

It can be observed that the emittance growth for O is very fast due to the QD error. After the initial blow-up during the first 1 000 turns, the emittance increase is slow or constant since the space charge effects are reduced due to the decreased particle density. An example of the tune spread for the O beam in the slice-by-slice model is given in Fig. 9. At injection (top left), the tune spread is large. When considering the ideal lattice, the emittance growth is small, and the tune footprint changes hardly after 2 000 turns (top right). In the case of the quadrupole error (bottom), where the emittance increases rapidly in the beginning, the tune spread reduces quickly, and is much smaller after 2 000 turns than after the same number of turns in the ideal case.

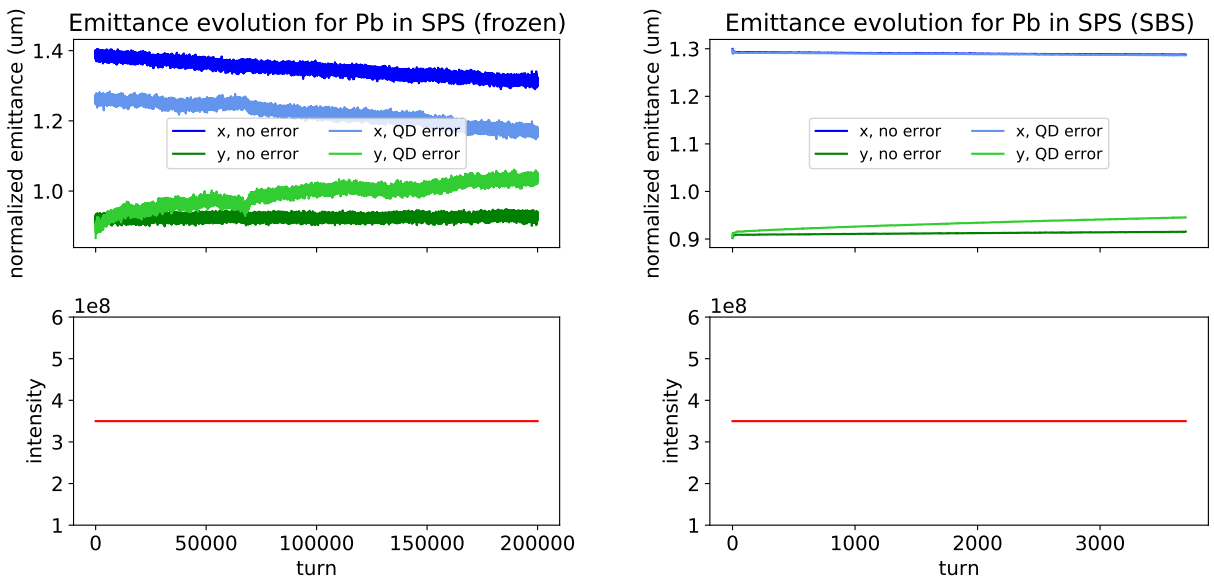


Figure 7: Simulation of the Pb beam in the frozen model (left) and the slice-by-slice model (right) case, comparing the emittance evolution of the ideal lattice with the QD error.

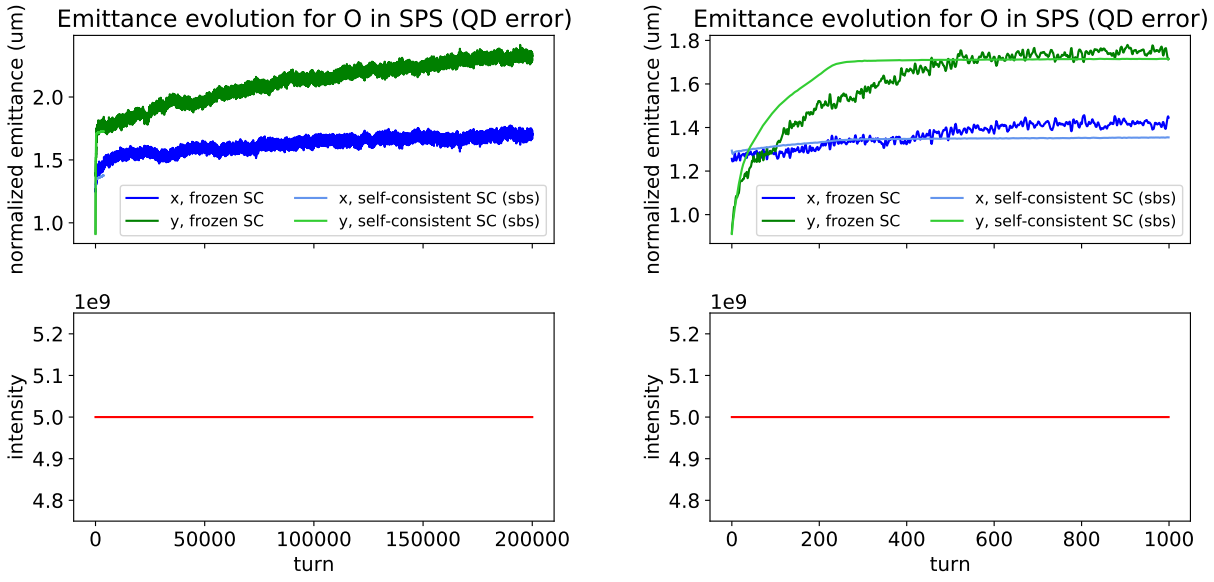


Figure 8: Emittance evolution for the O beam with quadrupole error. The left plot shows the full number of turns, the right plot focuses on the first 1 000 turns.

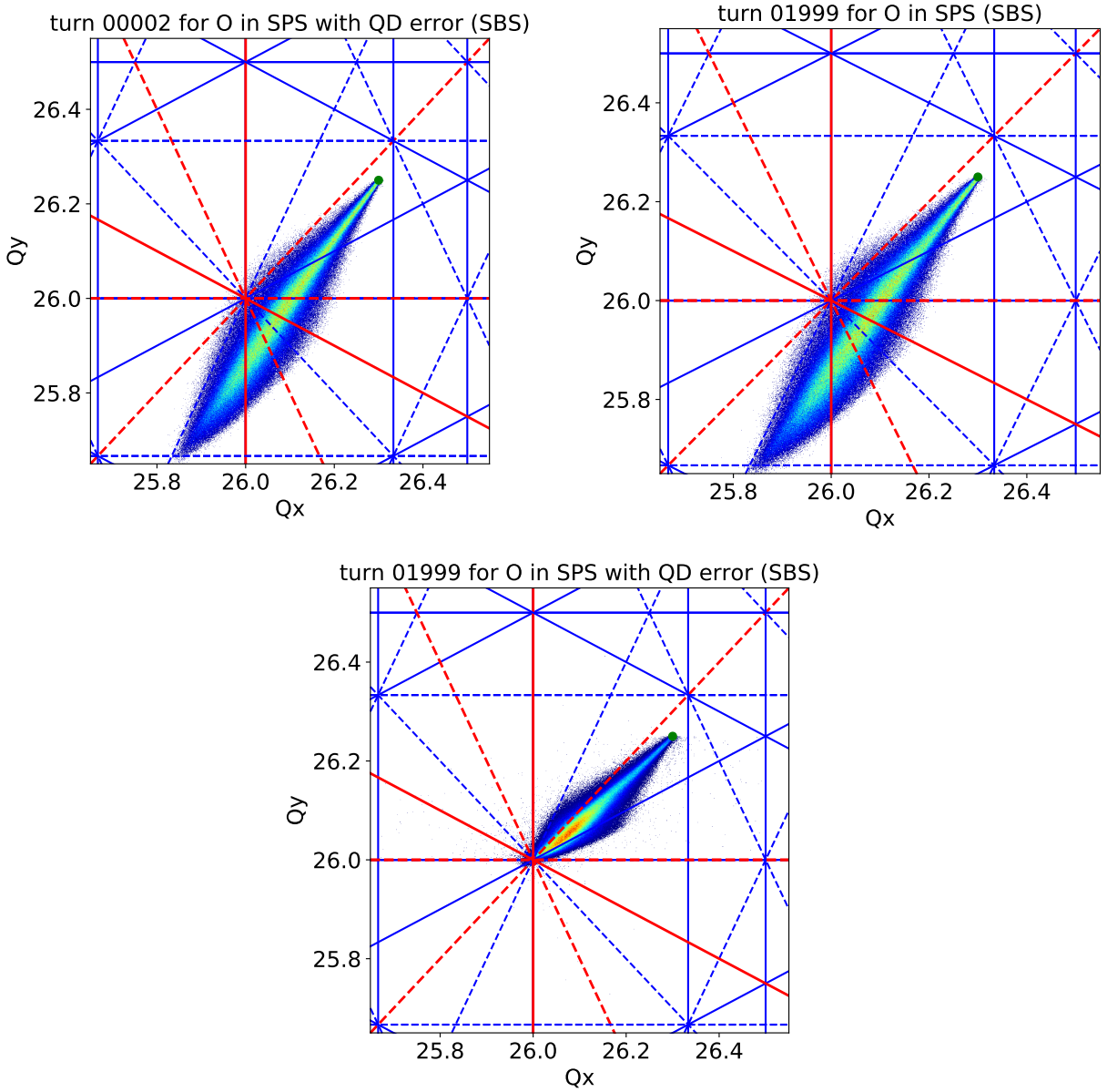


Figure 9: Evolution of tune spread for the O beam for the slice-by-slice SC solver, showing the tune footprint just after injection (top left), the tune footprint after 1 999 turns for the ideal lattice (top right), and the tune footprint after 1 999 turns for the lattice containing the quadrupole error (bottom).

# 3 Intrabeam scattering effects

In this section, the effects on the emittance and bunch length from intrabeam scattering are calculated for LEIR, PS and SPS, for both Pb and O beams.

## 3.1 Intrabeam scattering

Intrabeam scattering (IBS) refers to small angle Coulomb scattering between the particles inside a bunch of charged particles [4]. These particle collisions can affect the transverse emittances and the bunch length.

The IBS calculations are numerically done with the IBS module available in MAD-X [6] and compared to analytical calculations using the Nagaitsev method [7, 8]. All figures discussed below show the results from MAD-X as well as from the calculations using the Nagaitsev method, and the two methods give similar results. The input parameters are given in Table 2, and all other parameters are taken as in Table 1. For all injectors, the O beam is an "early" type beam produced by a single injection from Linac3 into LEIR, while the Pb is a "nominal" type beam produced from seven injections from Linac3 into LEIR [9].

Table 2: Input parameters for the IBS calculations for the different accelerators.

| | LEIR | PS | SPS |
|---|---|---|---|
| step size, $dt$ [s] | 0.01 | 0.01 | 0.1 |
| total time, $t$ [s] | 1 | 1 | 40 |
| $h$ | 2 | 16 | 4653 |
| $V_0$ [GV] | $1.1 \times 10^{-6}$ | $2.4 \times 10^{-5}$ (Pb)<br>$2.0 \times 10^{-5}$ (O) | $3.2 \times 10^{-3}$ |
| $\gamma_{\text{trans}}$ | 2.84 | 6.12 | 22.94 |
| $Q_h$ | 1.82 | 6.21 | 26.30 |
| $Q_v$ | 2.72 | 6.245 | 26.25 |

## 3.2 IBS in LEIR

For LEIR, a time period of 1 s after beam capture is considered (which is much longer than the beam storage at injection energy in LEIR, but is merely used for comparison between the two beam types). The results can be found in Fig. 10, while the relative emittance growths and bunch lengths are compared in Fig. 11. As expected, the emittance growth is much higher in the horizontal plane than in the vertical plane. The emittance growth for O is much smaller compared to the Pb beam, for which the horizontal blow-up reaches $> 250\%$. For O, IBS effects are therefore not expected to be a limitation as the operationally demonstrated beam parameters with Pb result in much higher IBS growth rates.

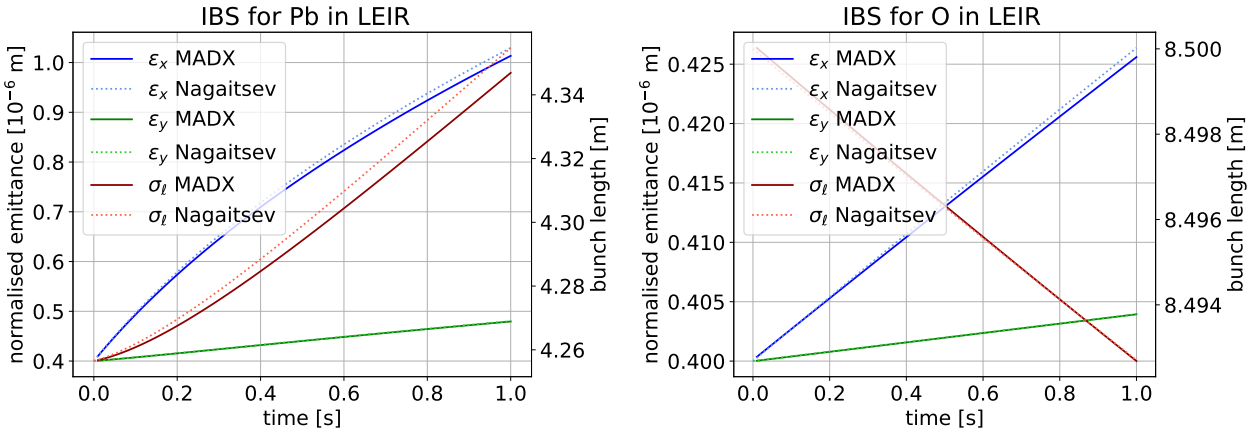


Figure 10: Emittances and bunch lengths for Pb (left) and O (right) in LEIR.

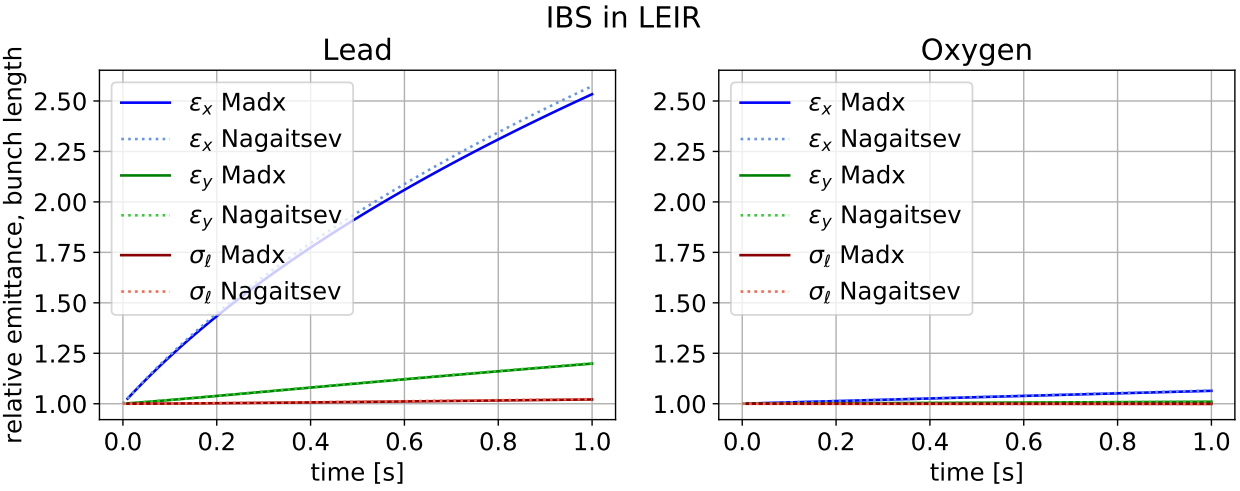


Figure 11: Emittance growth due to IBS for Pb and O in LEIR.

## 3.3 IBS in PS

For the PS, a time period of 1 s after injection is considered (this time period is used for comparison of the two beam types, the actual storage time at injection energy is much smaller in the operational ion cycle of the PS). Figure 12 shows the evolution of the transverse emittances and the bunch length. Figure 13 shows the effect of IBS on the relative transverse emittance and bunch length for Pb and O in PS. It can be observed that the emittance growth for O in the PS is very small – below $< 1\%$. This is much smaller than for Pb. Therefore, IBS effects are not expected to be a limitation for O beams in the PS since they are not even of concern for the operational Pb beams.

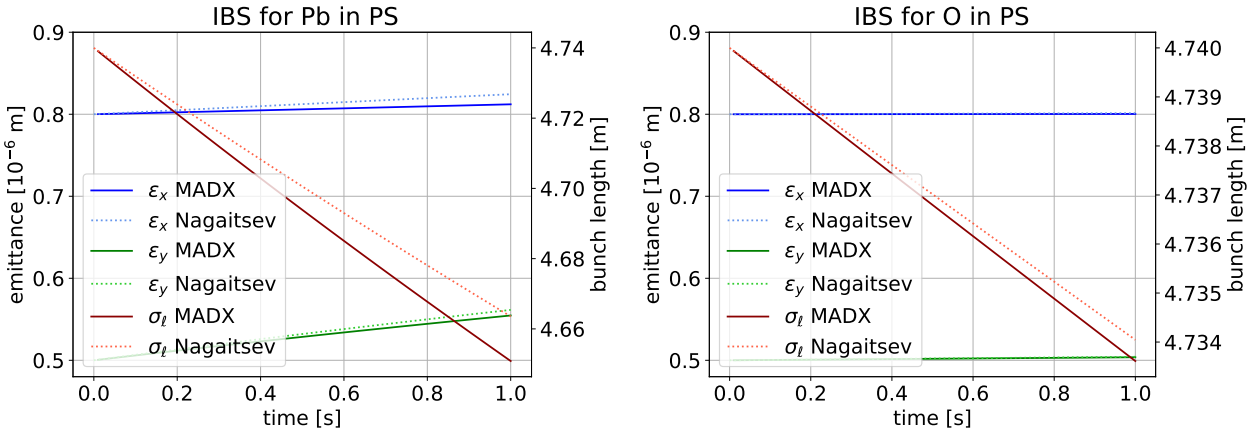


Figure 12: Transverse emittances and bunch length of Pb and O for PS.

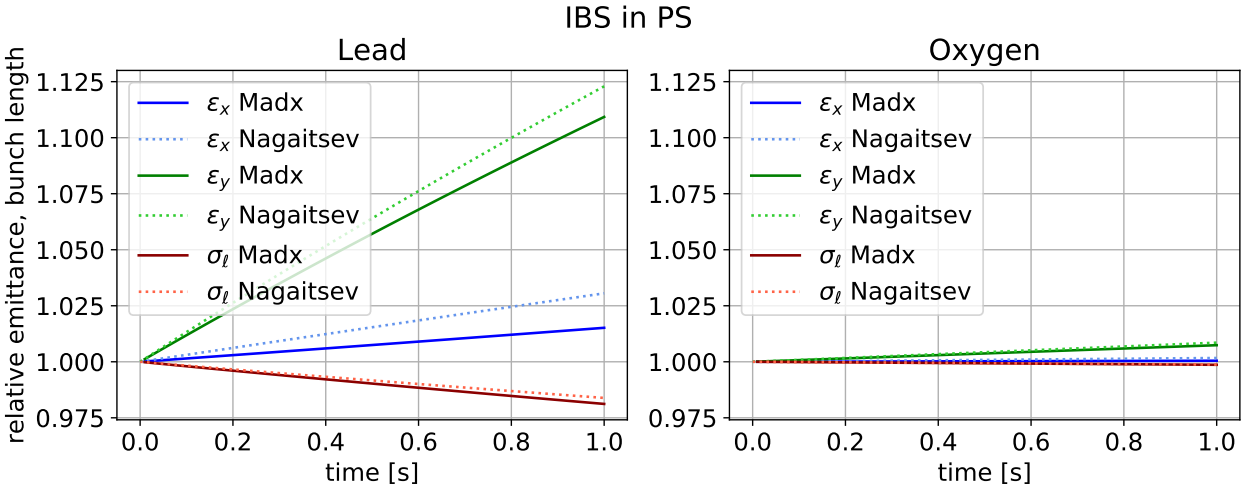


Figure 13: Emittance growth due to IBS for Pb and O in PS.

## 3.4 IBS in SPS

In the case of the Pb beam in the SPS, there are several injections of the bunches, and thus the beam has to be stored for approximately 40 s. However, since for O only a single injection will be used, the O beam does not have to be stored as long (typically less than 0.5 s before the start of the ramp). Nevertheless, for comparison with the Pb beam, a time period of 40 s is considered. Figure 14 shows the effect of IBS on the relative emittance and bunch length for Pb and O in SPS. In the SPS, the emittance growth for O due to IBS is still smaller than for Pb, and furthermore the beam will not be stored for a long time in the SPS. Thus IBS is not expected to be a limitation for O beams.

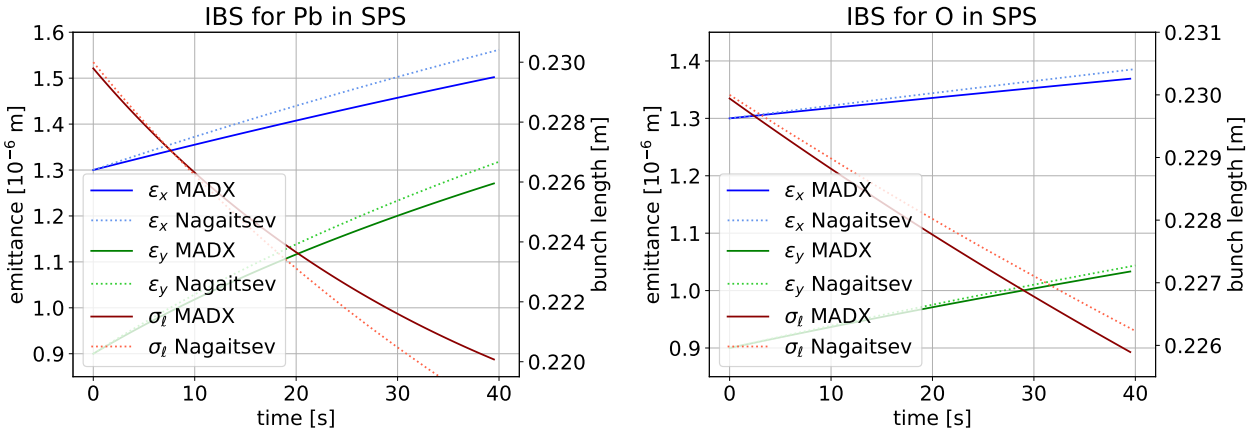


Figure 14: Comparison of the transverse emittance and bunch length obtained with MADX and the analytical calculation based on the Nagaitsev method for Pb (left) and O (right).

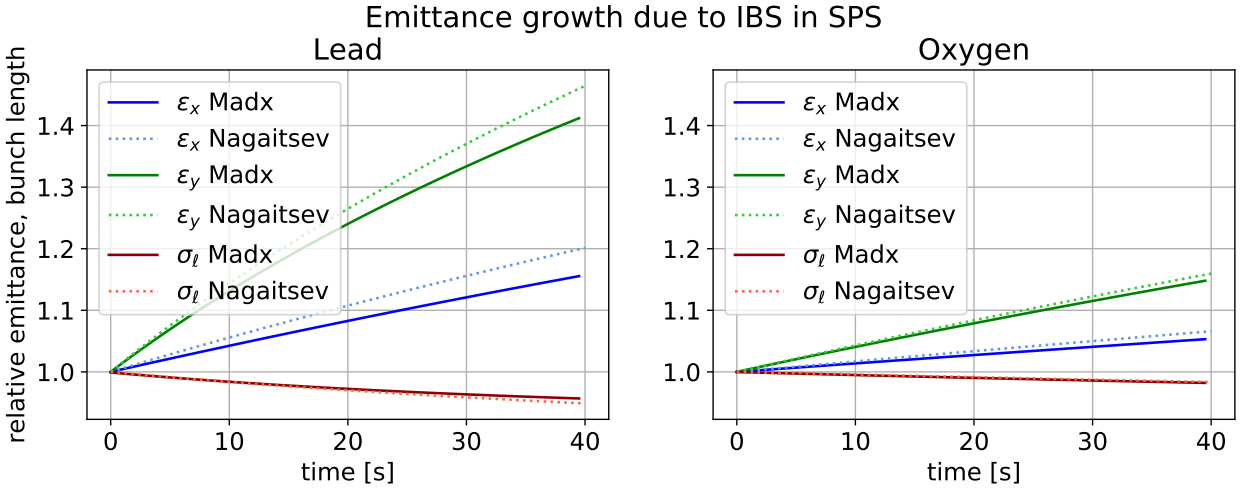


Figure 15: Relative emittances and bunch length of Pb and O for SPS.

As can be seen in Figs. 10 to 15, the results from the numerical MAD-X and analytical Nagaitsev calculation agree well with each other.

# 4 Comparison to experimental data

Measurements of the emittance evolution of Pb beams in the SPS have been performed in 2016, as presented at the Injector MD days in 2017 [10]. This data set is used for a comparison with the emittance evolution obtained from space charge simulations, as well as the emittance growth calculated from intrabeam scattering, using the methods described in Sections 2 and 3, respectively. In the space charge simulations, the same quadrupole error as previously is included. The parameters of the experimental setup from 2016 is given in Table 3. There were two configurations of the Pb beam with different initial emittances and

intensities. In case 1, the Beam Gas Ionisation Monitor (BGI) was used to measure the transverse profiles, while in case 2 the profile measurements were performed with the wire scanners (WS). The transverse emittances are obtained considering the beta functions at the respective instrument as provided by the SPS optics model.

Table 3: Emittance and number of ions at injection, used during the beam measurements in 2016.

| | $\varepsilon_x$ [$10^{-6}$ m] | $\varepsilon_y$ [$10^{-6}$ m] | $N_{\text{ions}}$ [$10^8$ ions/bunch] |
|---|---|---|---|
| case 1 | 1.7 | 0.95 | 3.5 |
| case 2 | 2.5 | 0.95 | 2.6 |

The measurements are presented in Fig. 16. The beam emittance growth is caused by space charge and intrabeam scattering, and possibly other effects that still need to be identified.

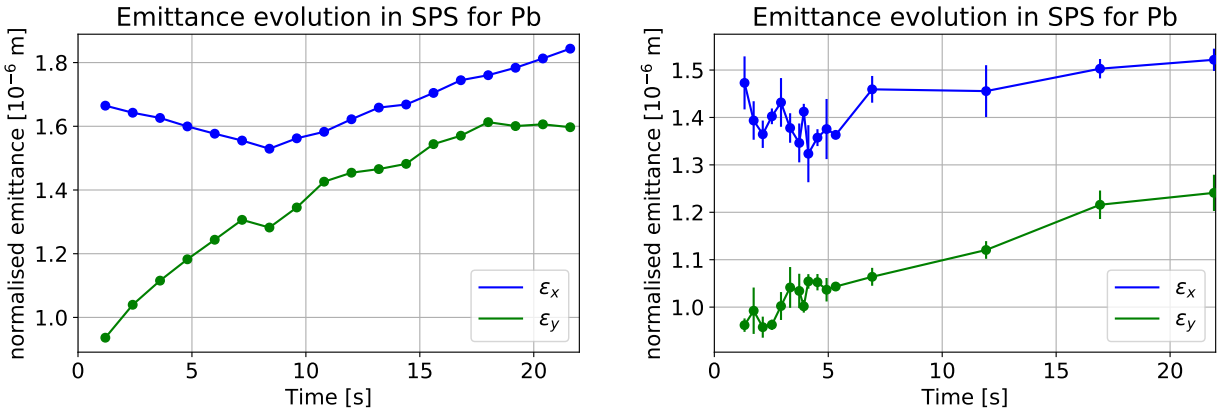


Figure 16: Emittance evolution along the flat bottom measured with the BGI for a bunch intensity of $3.5 \cdot 10^8$ Pb ions/bunch at injection (left), and measured with the WS for a bunch intensity of $2.6 \cdot 10^8$ Pb ions/bunch at injection (right). Plots taken from [10].

Figure 17 shows the emittance evolution obtained in SC simulations compared to the emittance evolution considering only IBS, and in comparison to the measurements from 2016.

Similarly, Fig. 18 shows the same results from the measurements and SC and IBS calculations, but to get a better picture of the overall emittance evolution, the average transverse emittances are shown, given by $(\varepsilon_x + \varepsilon_y)/2$. The right plot in Fig. 18 also shows the propagation of the error in the measurements.

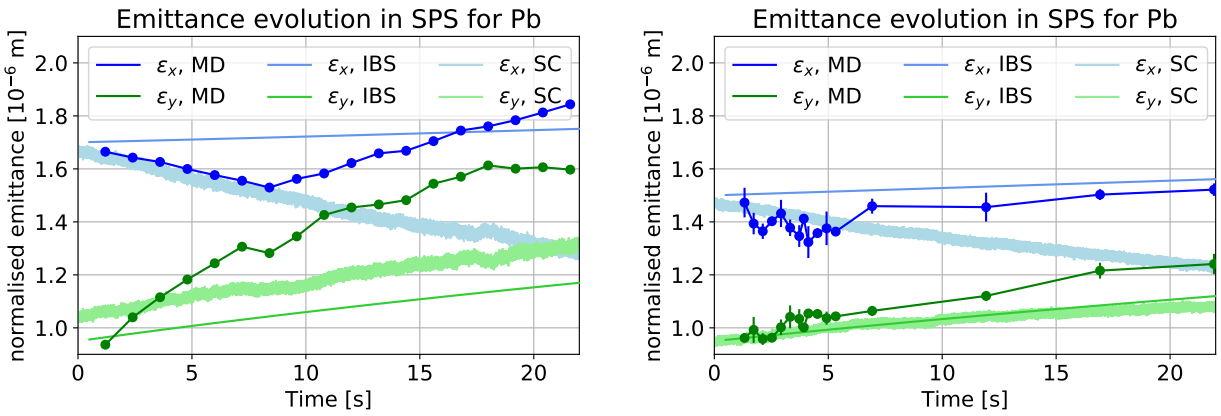


Figure 17: Emittance evolution from the 2016 measurements, due to SC effects and due to IBS effects for case 1 (left) and case 2 (right).

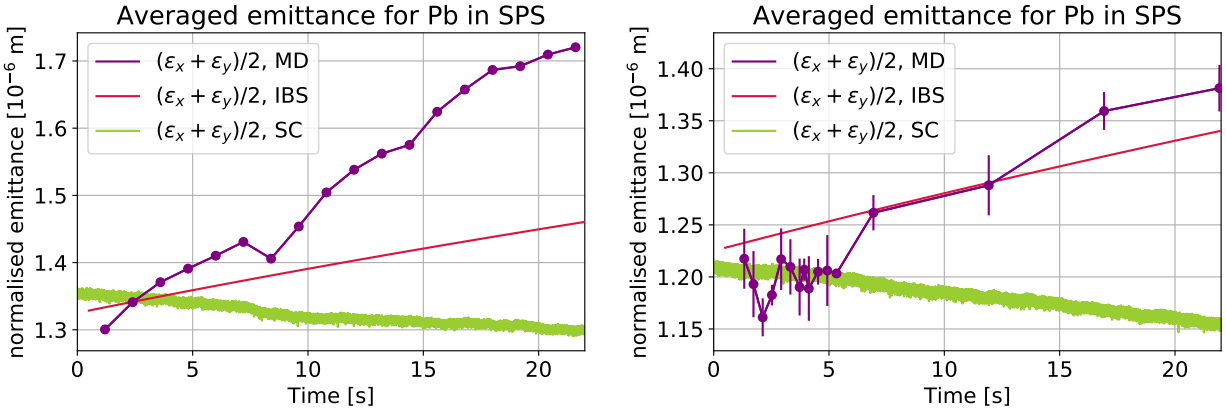


Figure 18: Averaged emittance evolution from the MD 2017 measurements, due to SC effects and due to IBS effects for case 1 (left) and case 2 (right).

Overall, the contribution from IBS results in a growth in the transverse emittance, while from the space charge effects alone an average decrease in the transverse emittance due to exchange with the longitudinal emittance is observed. In the measurements, the emittance increase is larger than the one observed from IBS, especially in case 1 (left plot). The measurements in case 1 were taken with the BGI which gives less accurate results than the WS, used in case 2 (right plot). It is clear that the simulation results do not reproduce the emittance growth observed in the measurements. At the moment, the interplay between space charge and intrabeam scattering effects has not been studied, since calculations and simulations of the emittance evolution are done separately for space charge or intrabeam scattering (due to limitations in the simulation tools used for these studies). Furthermore, in the measurements, other effects might play an important role that have not been considered here.

Table 4: Available aperture in units of beam $\sigma$ for the Pb beam and the O beam in the SPS, given for the injection emittance and the doubled emittance.

| | $\varepsilon_x$ [$10^{-6}$ m] | $\varepsilon_y$ [$10^{-6}$ m] | number of $\sigma_x$ | number of $\sigma_y$ |
|---|---|---|---|---|
| Pb | 2.6 | 1.8 | 7.1 | 4.3 |
| O | 1.58 | 1.82 | 8.4 | 4.2 |

# 5 Aperture considerations for SPS

In this section, the beam size of the Pb and O beams are compared to the aperture of the SPS to determine possible limitations for the beam after emittance blow-up.

From the measurements shown in Fig. 16, it can be concluded that the emittance of the Pb beam after about 22 s storage in the SPS can be estimated to have blown up by a factor of two in the vertical plane and less in the horizontal plane. Similarly, for the O beam from the simulations (see e.g. Fig. 8), it can be observed that the vertical emittance roughly doubles. Therefore, the doubled injection emittance is a good estimate for the blow-up of the (vertical) emittance, and this can be used to determine how the increased emittance compares to the aperture of the accelerator. This investigation is especially interesting for the O beam, since the tune shift is large ($\approx -0.55$ in the vertical plane). As the emittance increases accordingly, the beam size could become larger than the available machine aperture resulting in particle losses.

The transverse beam sizes in the horizontal and vertical planes are calculated using Eq. 2. For each element of SPS, the size of the (half-) aperture $a$ is divided by the beam size $\sigma$ to determine the space available for the beam in terms of beam size, i.e. $a_{x,y}/\sigma_{x,y}$. Since there are other effects that can increase the emittance that are not taken into account here, a minimum of about $5\sigma$ is considered sufficient to avoid beam losses. In these calculations, no closed orbit errors are assumed.

The number of $\sigma$ for the position of each element in the SPS is shown in Figs. 19 and 20 for the Pb beam and the O beam, respectively. For the O beam, the emittances from the 2.5D simulation with the quadrupole error after 10 000 turns are used. As can be seen in the top plots, in the horizontal plane for both the Pb beam and the O beam, the number of $\sigma$ is well above 5, and thus no limitations are expected. However, in the vertical plane shown in the bottom plots, the number of $\sigma$ is below 5. For the Pb beam, this could explain part of the beam losses observed in the real machine. For the O beam, as the situation is very similar to the one of the Pb beam, the O beam might suffer from losses as well. A summary with the minimum $\sigma$ in each case is given in Table 4.

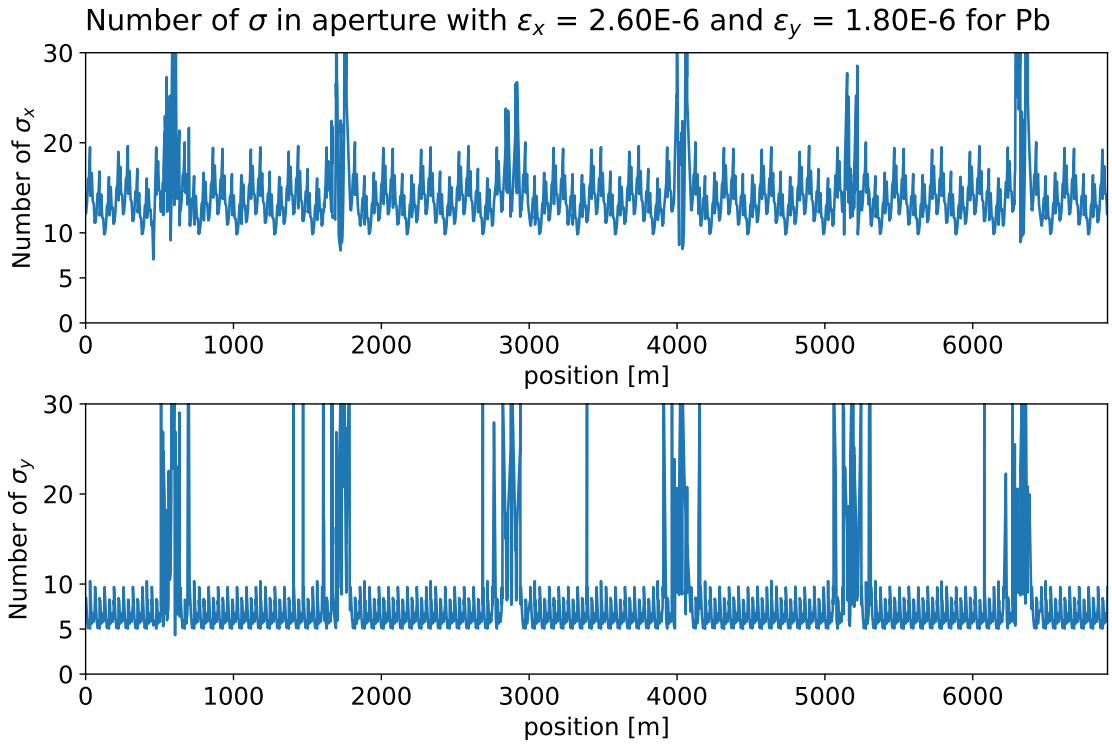


Figure 19: Number of $\sigma$ in aperture for the Pb beam in the SPS for twice the injection emittances.

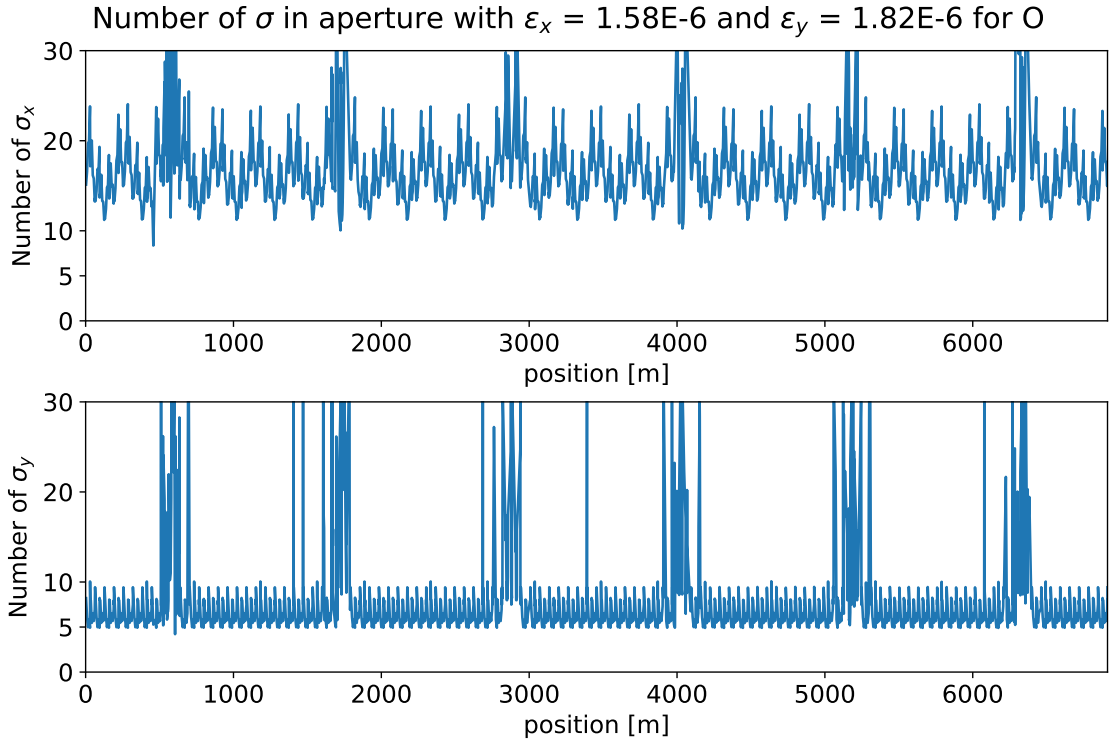


Figure 20: Number of $\sigma$ in aperture for the O beam in the SPS for roughly twice the injection emittances.

# 6 Summary and conclusions

Table 5 summarises all parameters for the Pb beam and the O beam in the LHC injector chain (LEIR, PS and SPS), including the analytically calculated tune shifts from SC and the relative transverse emittance growth rate from IBS, given by $\varepsilon\,(1\text{ s})\,/\varepsilon\,(0)$ for 1 s.

In LEIR and PS, the SC tune shift is smaller for the O beam than for the Pb beam. Also, the emittance growth due to IBS is much smaller for the O beam than for the Pb beam. Therefore, based on the operational experience with the Pb beam, no limitations for the O beam are expected in LEIR and PS. In the SPS, the SC tune shift is large for the O beam. A very fast emittance blow-up is expected from the simulations, that is also relevant for single injections. This might result in losses on the aperture. For IBS, the emittance growth is smaller for the O beam than for the Pb beam, and IBS is therefore not expected to be a limitation in the SPS.

Overall, the only limitation for the O beam in the LHC injector chain may arise from SC effects in the SPS, potentially causing losses on the aperture on a similar scale as already observed for the Pb beam. To avoid these losses, it might be preferable to perform a bunch splitting of the O beam in the PS, so that the intensity per bunch is halved in the SPS. This would eliminate losses caused by the SC induced blow-up, as the tune spread would be comfortably within the operational values of the Pb beam. For completeness, this variant of the O beam is also included in the summary given in Table 5. It should be noted however that the impact on the luminosity reach in the LHC using a beam with lower bunch intensity would need to be evaluated.

Table 5: Summary of all input parameters used in the calculations and simulations, as well as the obtained analytical tune shifts due to space charge effects, and the relative emittance growth caused by intrabeam scattering.

| | | LEIR | | PS | | SPS | | |
|---|---|---|---|---|---|---|---|---|
| | | Pb | O | Pb | O | Pb | O | |
| | $\varepsilon_x$ [$10^{-6}$ m] | 0.4 (3) | 0.4 (4) | 0.8 (2) | 0.8 (4) | 1.3 (3) | 1.3 (4) | 1.3 |
| | $\varepsilon_y$ [$10^{-6}$ m] | 0.4 (3) | 0.4 (4) | 0.5 (2) | 0.5 (4) | 0.9 (3) | 0.9 (4) | 0.9 |
| | $\Delta p/p$ [$10^{-3}$] | 1.18 | 1.18 (4) | 0.63 | 0.63 (4) | 1 | 1 (4) | 1 |
| | $N_b$ [$10^8$] | 10 (2) | 110 (1) | 8.1 (2) | 88 (1) | 3.5 (2) | 50 (1) | 25 |
| | $n_q$ | 54 (2) | 4 (1) | 54 (2) | 4 (1) | 82 (2) | 8 (1) | 8 |
| | $\sigma_z$ [m] | 4.256 | 8.5 (4) | 4.74 | 4.74 (4) | 0.23 | 0.23 (4) | 0.23 |
| | $E_{\mathrm{kin}}/u$ [GeV] | 0.0042 (2) | 0.0042 (1) | 0.072 (2) | 0.0672 (1) | 5.9 (2) | 5.63 (1) | 5.63 |
| | $m$ [GeV] | 193.8 | 14.9 | 193.8 | 14.9 | 193.8 | 14.9 | 14.9 |
| | $B\rho$ [Tm] | 1.14 | 1.18 | 4.81 | 4.81 | 57.4 | 43.4 | 43.4 |
| | $\beta$ | 0.09464 | 0.09464 | 0.3720 | 0.3606 | 0.9907 | 0.9899 | 0.9899 |
| | $\gamma$ | 1.00451 | 1.00451 | 1.0773 | 1.07214 | 7.33391 | 7.04405 | 7.04405 |
| SC | $\Delta Q_x$ | −0.35 | −0.14 | −0.24 | −0.19 | −0.20 | −0.38 | −0.19 |
| SC | $\Delta Q_y$ | −0.31 | −0.12 | −0.3 | −0.24 | −0.29 | −0.55 | −0.28 |
| IBS | $\varepsilon_x/\varepsilon_{x,0}$ in 1 s | 2.4712 | 1.0631 | 1.0150 | 1.0005 | 1.0044 | 1.0014 | – |
| IBS | $\varepsilon_y/\varepsilon_{y,0}$ in 1 s | 1.1967 | 1.0098 | 1.1080 | 1.0073 | 1.0145 | 1.0042 | – |

References:

(1) ref. [1]

(2) ref. [2]

(3) ref. [5]

(4) if not known for O, assuming same as for corresponding Pb beam

# References


[1] R. Alemany. *LHC Oxygen pilot run in Run 3: Injectors perspective*. https://indico.cern.ch/event/863134/contributions/3637254/attachments/1943751/3224358/Oxygen_pilot_run_equipment_groups.pdf.

[2] *LIU ions beam parameter table, EDMS:1420286*. https://edms.cern.ch/document/1420286/.

[3] K. Wille and J. McFall. *The Physics of Particle Accelerators: An Introduction*. The Physics of Particle Accelerators: An Introduction. Oxford University Press, 2000. ISBN: 9780198505495.

[4] Karlheinz Schindl. "Space charge". In: *CAS - CERN Accelerator School: Intermediate Course on Accelerator Physics* (2006). DOI: 10.5170/CERN-2006-002.305. URL: https://cds.cern.ch/record/941316.

[5] A. Huschauer. *Pb ion emittance evolution across the injector chain. Presentation at the LHC injector MD days 2017*. CERN, 2017, https://indico.cern.ch/event/609486/contributions/2457575/attachments/1433312/2203103/Ions_emittance_evolution_MD_days.pdf.

[6] *MAD – Methodical Accelerator Design*. https://mad.web.cern.ch/mad/.

[7] M. Zampetakis. *Private communication*.

[8] Sergei Nagaitsev. "Intrabeam scattering formulas for fast numerical evaluation". In: *Phys. Rev. ST Accel. Beams* 8 (6 June 2005), p. 064403. DOI: 10.1103/PhysRevSTAB.8.064403. URL: https://link.aps.org/doi/10.1103/PhysRevSTAB.8.064403.

[9] M. Benedikt et al. *LHC Design Report*. CERN Yellow Reports: Monographs. Geneva: CERN, 2004. DOI: 10.5170/CERN-2004-003-V-3. URL: https://cds.cern.ch/record/823808.

[10] A. Saa Hernandez et al. *Transverse studies with ions at SPS flat bottom. In Proceedings of Injector MD Days 2017*. Geneva: CERN, 2017. DOI: 10.23727/CERN-Proceedings-2017-002. URL: https://cds.cern.ch/record/2300752.

# A Comparison of the simulation models

In this section, the three simulation models used in this work are compared by considering the emittance evolution, tune spread evolution and transverse mean position of the beam.

**Frozen space charge solver**

The frozen model is based on the assumption that the transverse particle distribution is Gaussian, centered around the closed orbit. Therefore, a small number of macroparticles (around 1 000) is sufficient to simulate the beam evolution, which makes the computation time shorter. A limitation of the frozen model is that it is not self-consistent since the bunch profiles are assumed to always be Gaussian, even when they are not.

**2.5D self-consistent space charge solver**

The 2.5D self-consistent model requires more macroparticles than the frozen model, and therefore the computation time is increased. In this model all transverse coordinates are treated together when calculating the space charge kick through a Particle-In-Cell (PIC) algorithm, but the strength of the kick changes according to the longitudinal position. The standard grid size is (64, 64, 32), i.e. 64 by 64 cells in the transverse grid and 32 longitudinal slices.

**Slice-by-slice self-consistent space charge solver**

In the slice-by-slice self-consistent space charge solver, the transverse coordinates of the bunch are treated slice by slice (longitudinally) with a total grid size of (128, 128, 64). This method requires a large amount of macroparticles to resolve the particle distribution ($\approx 1\,000\,000$), which leads to a long computation time.

For comparison of the simulation times needed for the different solvers available, the following examples can be considered. The frozen simulations for 200 000 turns take several hours (around 7), using one node (consisting of 20 CPUs) at the CERN HPC cluster. The 2.5D simulations for 10 000 turns take a couple of days, using one node. The slice-by-slice simulations for about 4 000 turns take about a week, using two nodes (thus a total of 40 CPUs).

## A.1 Emittance evolution

**Frozen model with more macroparticles**

In the results shown previously for the frozen model, the number of macroparticles is 1 000. In Fig. 21, this is compared to 50 000 macroparticles for the emittance evolution for the O beam including the quadrupole error. As can be seen, the graph becomes smoother when introducing more particles, but overall the emittance evolution is the same. This comparison justifies using only a small number of macroparticles (e.g. 1 000) for the frozen space charge model.

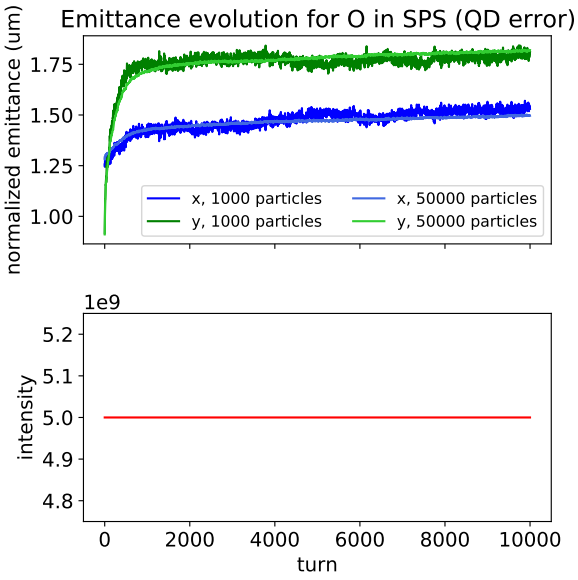


Figure 21: Emittance evolution of the O beam with a QD error for the frozen model with 1 000 and 50 000 macroparticles.

#### Comparison between 2.5D and slice-by-slice models

As shown in Section 2, the frozen model and the slice-by-slice model give similar results of the emittance evolution within the limitation of the methods. In Fig. 22, the emittance evolution for O is compared for the 2.5D and slice-by-slice model, in the ideal case (left) and the case with a quadruple error (right). In both models a small emittance increase (mostly in the vertical direction) is observed in the ideal case, and a very fast emittance blow-up for the case with the quadrupole error. It can be observed that, in the long term, the emittance keeps increasing steadily in the 2.5D model with a higher rate compared to the slice-by-slice model. This is most likely caused by an artefact of the 2.5D solver (as the transverse space charge kicks are computed by taking into account all transverse macroparticle positions at the same time instead of calculating the potential for each longitudinal slice individually) and is thus believed to be an artificial emittance growth. On the other hand, the slice-by-slice model shows a more stable emittance evolution, which is probably more realistic.

## A.2 Tune diagrams

For some of the 2.5D simulation cases, the tune diagram acquires an unexpected shape after several 1 000 turns, as shown in Fig. 23. In the right plot, the tune spread does not have the typical shape that is still visible in the left plot showing the tune spread after about 100 turns. This unusual shape is likely due to an artificial, large spread in the transverse position of the beam that is further discussed in the next section (Section A.3).

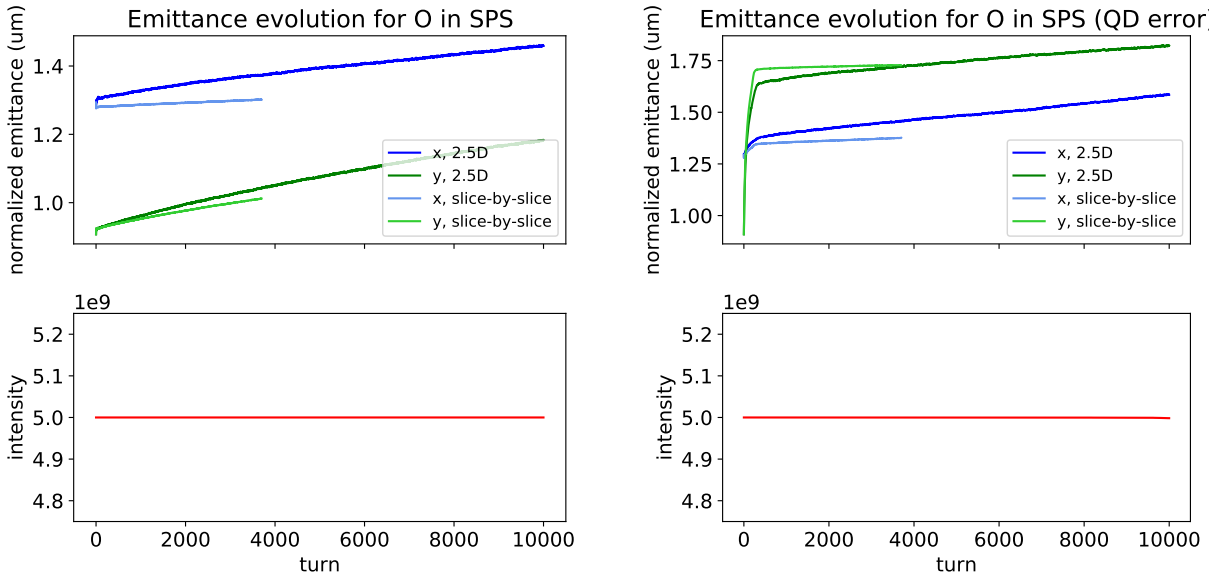


Figure 22: Comparison of the 2.5D and slice-by-slice self-consistent space charge models, for the ideal lattice (left) and the quadrupole error (right) for the O beam.

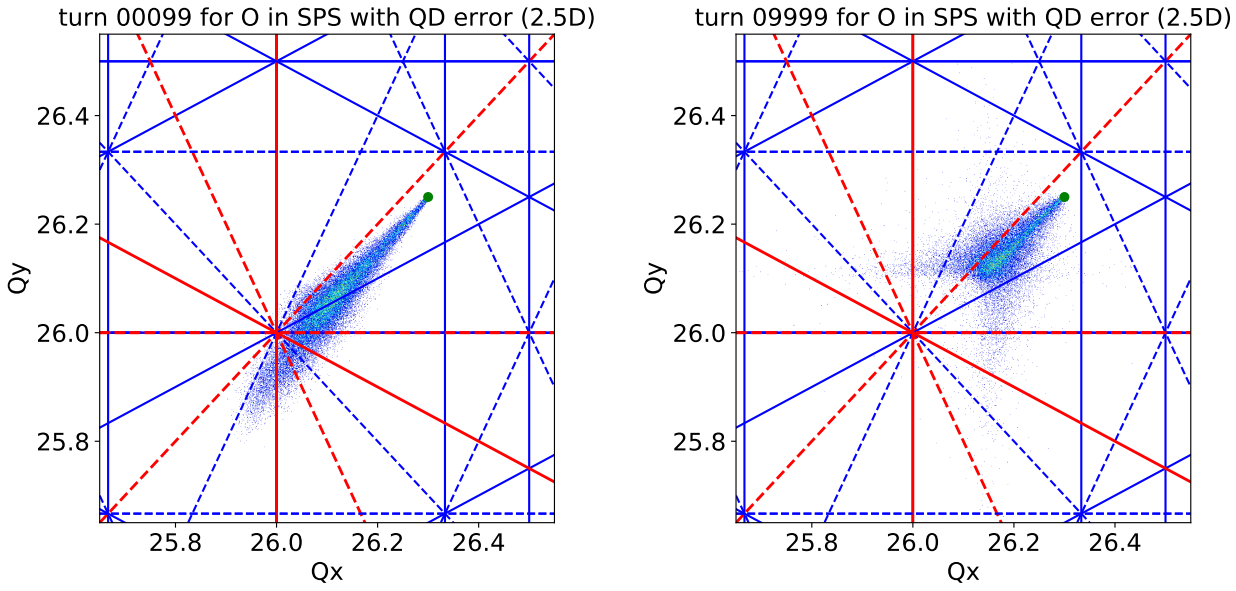


Figure 23: Injection (left) and later (right) tune footprint for the O beam in the 2.5D model.

## A.3 Mean transverse beam position

Figure 24 shows the mean transverse position of the beam for the self-consistent simulation models for the O beam with quadrupole error. It can be observed that the mean transverse position increases along the simulation in the 2.5D model. For the slice-by-slice model, the transverse mean position is much more stable and only changes with a small amplitude, as

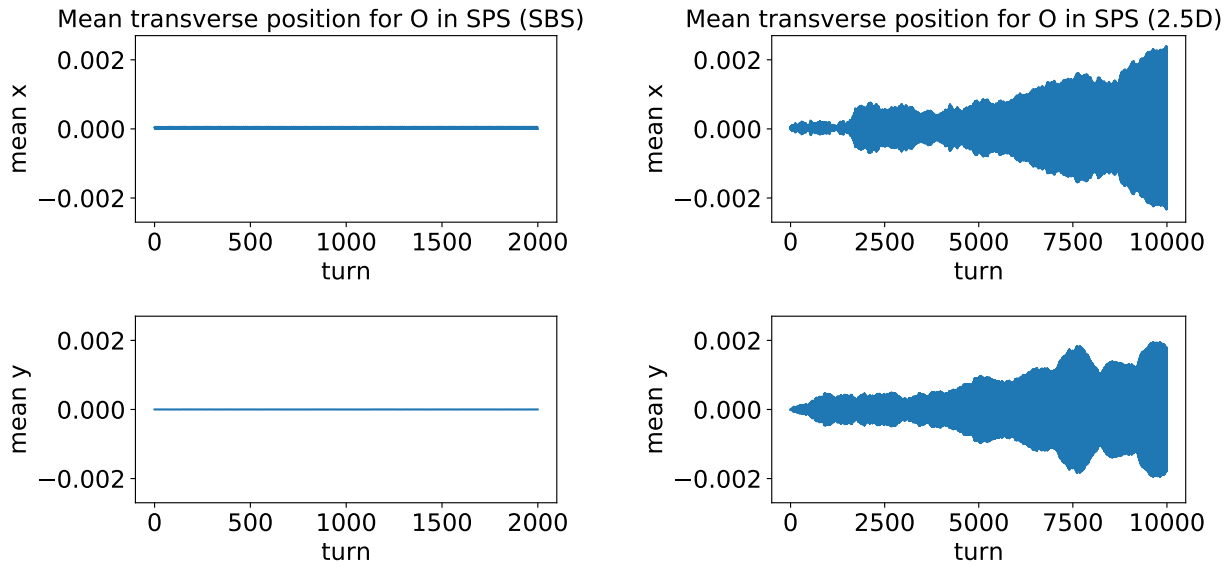


Figure 24: Mean transverse position of the particles per turn for the two self-consistent simulation models: slice-by-slice (left) and 2.5D (right).

expected in the machine.

For the 2.5D model, increasing the number of macroparticles from 100 000 to 500 000, as well as also increasing the grid size from (64, 64, 32) to (128, 128, 64) has reduced the artificial growth of the beam bunch positions, as shown in Fig. 25. The top left plot shows the simulation with 100 000 macroparticles, displaying the largest spread and growth. The top right plot shows the transverse mean position with the smallest spread where the number of macroparticles is increased to 500 000. When also increasing the grid size, as shown in the bottom plot, the spread in the transverse mean position increases again. This clearly demonstrates that the observed growth of the mean transverse bunch position is a numerical artefact of the simulation model. Therefore, the slice-by-slice model, which did not exhibit such an artefact, was considered as reference in the studies presented in this paper.

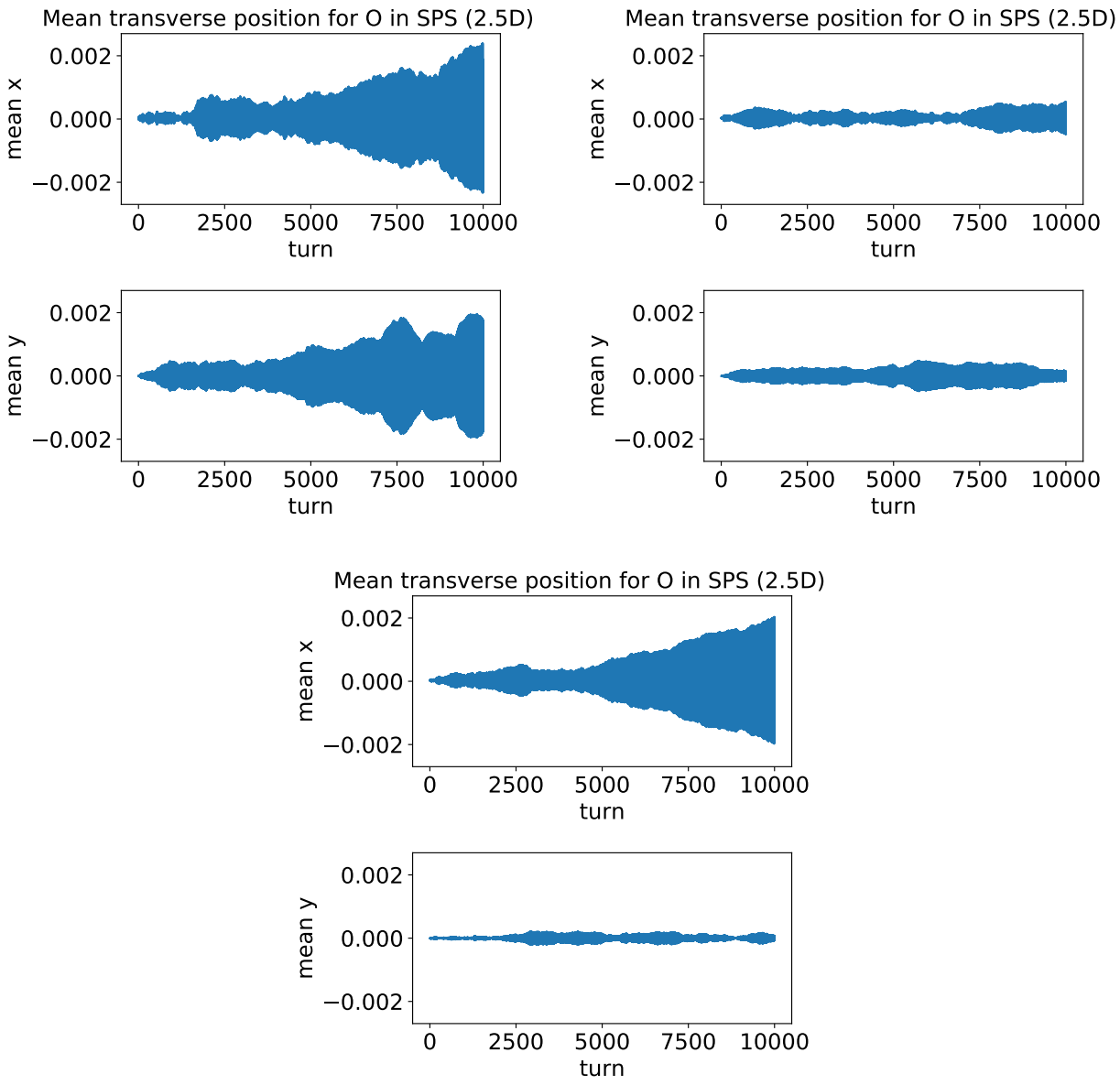


Figure 25: Mean transverse position of 2.5D simulation with 100 000 macroparticles (top left), 500 000 macroparticles (top right), and 500 000 and increased grid size (bottom).

# B Analytical tune shift compared to simulation

It was observed that the tune shifts obtained in the simulations do not always fit well with the analytically calculated tune shifts using Eq. 1 with the parameters for a specific turn. The discrepancy is especially large in the case of the quadrupole error. The reason for the discrepancy stems probably from the calculation of the tune shift using Eq. 1, which assumes a Gaussian distribution of the beam profiles. However, from the simulations it can be observed that the bunch profiles are not Gaussian when introducing a quadrupole error. An example of the bunch profiles after 200 000 turns for the frozen model are given in Fig. 26. While in the no error case (top) the bunch profiles in the transverse plane are close to a Gaussian, the case including the quadrupole error (bottom) shows a larger discrepancy from the Gaussian shape due to the blow-up on the half-integer resonance.

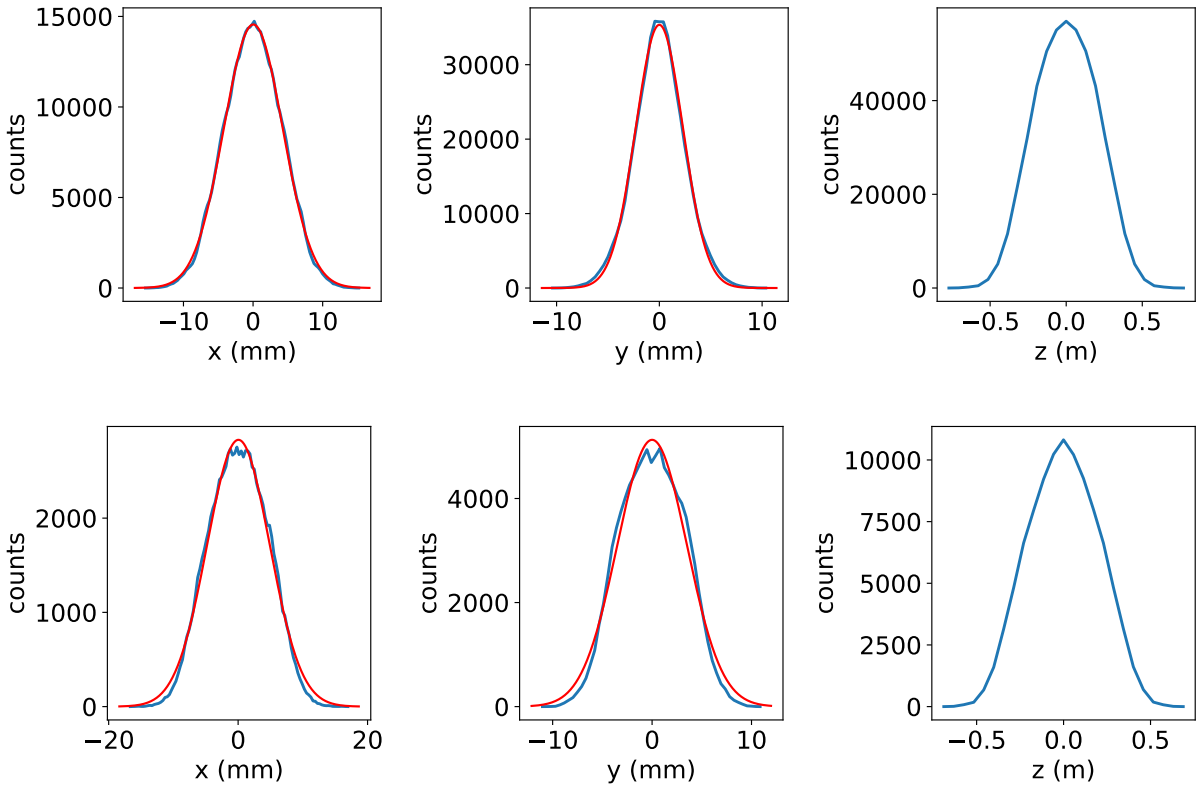


Figure 26: Bunch profiles for the frozen model with no error (top figures) and with QD error after (bottom figures) after 200 000 turns. Red curves indicate the Gaussian fit.

Table 6 shows a summary of the calculated tune shifts for different configurations of the simulations after a specific amount of turns, as indicated in the table. The first four cases, as indicated, are based on a Gaussian line density, as given in Eq. 1. For the other cases, as the longitudinal bunch profile does not follow a Gaussian distribution (for an example, see Fig. 27), a different approach is used. The following replacement is made:

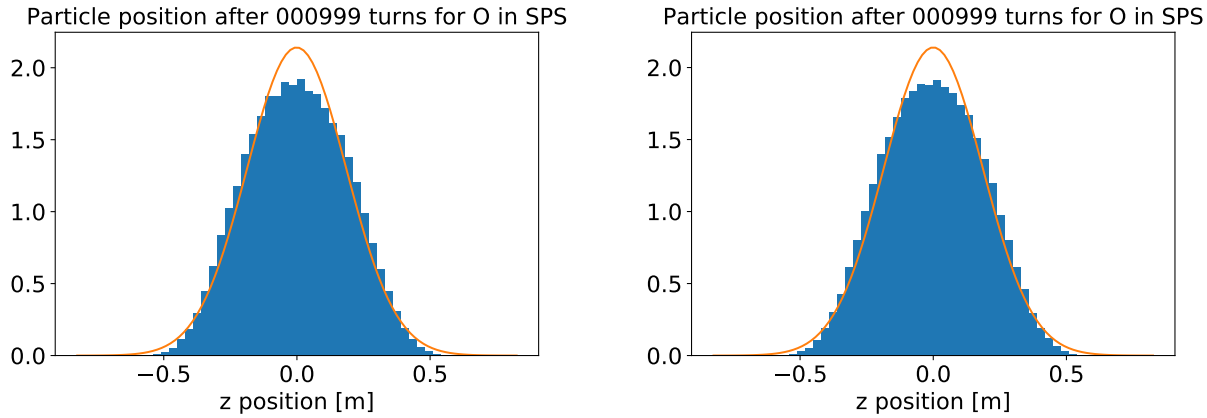


Figure 27: The longitudinal bunch profiles compared to a Gaussian fit (orange) for the 2.5D model with no error (left) and with QD error (right), for 999 turns.

$$\frac{1}{\sqrt{2\pi}\sigma_z} \rightarrow \frac{h}{2\pi R B_f}, \tag{3}$$

where $R$ is the radius of SPS ($R = 1100$ m), $h = 4653$ is the harmonic number used for ion beams at SPS injection, and $B_f$ is the bunching factor, given by $B_f = \bar{\lambda}/\hat{\lambda}$, where $\bar{\lambda}$ is the average line density for one RF bucket and $\hat{\lambda}$ is the peak line density in the center of the bunch. The bunching factor is determined by the longitudinal bunch profile of the corresponding turn: the sum of all bins divided by the number of bins, $\bar{\lambda}$, divided by the peak of the line density distribution, $\hat{\lambda}$. Examples are given in Fig. 28 for two tune footprints with the tune shifts calculated using Eq. 3. The tune shifts calculated like this show better agreement with the simulated results.

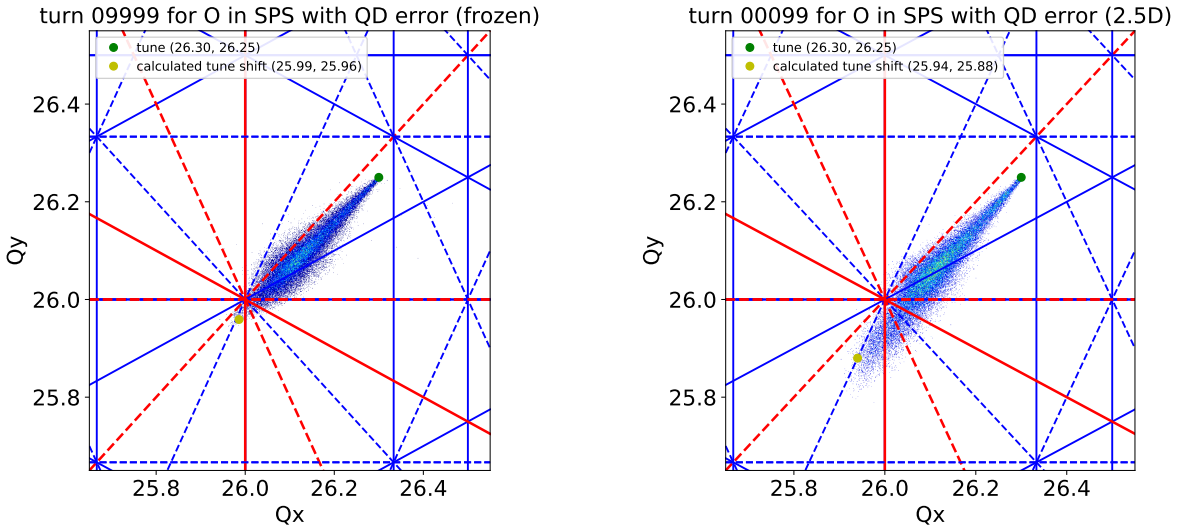


Figure 28: Tune footprints obtained from the simulations compared to the calculated tune shift. The left figure shows the tunes for the frozen model after 9 999 turns, while the right figure presents the tunes of the 2.5D model for 99 turns. The green dot indicates the bare tune, and the yellow dot the calculated shifted tune.

Table 6: Overview of all calculated tune shifts after a different number of turns. Where indicated, a Gaussian line density distribution is assumed. Otherwise, the calculation is made by replacing the Gaussian line density distribution by the actual bunching factor as given in Eq. 3.

| | macroparticles | turn | $\Delta Q_x$ | $\Delta Q_y$ | $Q_x$ | $Q_y$ |
|---|---|---|---|---|---|---|
| Pb, frozen (Gaussian) | 1 000 | 100 | −0.20 | −0.19 | 26.10 | 25.94 |
| O, frozen (Gaussian) | 1 000 | 100 | −0.33 | −0.55 | 25.97 | 25.70 |
| Pb, 2.5d (Gaussian) | 100 000 | 99 | −0.20 | −0.19 | 26.10 | 25.94 |
| O, 2.5d (Gaussian) | 100 000 | 99 | −0.33 | −0.55 | 25.97 | 25.70 |
| O, 2.5d | 100 000 | 99 | −0.397 | −0.499 | 25.90 | 25.75 |
| O, 2.5d | 100 000 | 9 999 | −0.377 | −0.440 | 25.92 | 25.81 |
| O, 2.5d | 500 000 | 99 | −0.424 | −0.532 | 25.88 | 25.72 |
| O, 2.5d | 500 000 | 999 | −0.421 | −0.523 | 25.88 | 25.73 |
| O, frozen, QD error | 1 000 | 99 | −0.373 | −0.391 | 25.93 | 25.86 |
| O, frozen, QD error | 1 000 | 199 999 | −0.295 | −0.260 | 26.01 | 25.99 |
| O, 2.5d, QD error | 100 000 | 99 | −0.364 | −0.371 | 25.94 | 25.88 |
| O, 2.5d, QD error | 100 000 | 999 | −0.339 | −0.324 | 25.96 | 25.93 |
| O, 2.5d, QD error | 100 000 | 9 999 | −0.307 | −0.297 | 25.99 | 25.95 |
| O, frozen, QD error | 50 000 | 99 | −0.371 | −0.392 | 25.93 | 25.86 |
| O, frozen, QD error | 50 000 | 9 999 | −0.314 | −0.295 | 25.99 | 25.96 |